Supplement of Atmos. Chem. Phys., 26, 8275–8294, 2026
https://doi.org/10.5194/acp-26-8275-2026-supplement

Atmospheric Chemistry and Physics Open Access

Supplement of

Ozone formation sensitivity based on the secondary formaldehyde-to-nitrogen dioxide ratio (FNR_{sec}) derived from ground-based remote sensing measurements and a chemical transport model

Nguyen Doan Thien Chi et al.

Correspondence to: Nguyen Doan Thien Chi (nguyen.doanthienchi@nies.go.jp) and Hiroshi Tanimoto (tanimoto@nies.go.jp)

Table S1: The Pandora stations used in this study

Location name	Latitude (deg)	Longitude (deg)	Instrument number	Location altitude (m)	Local Operator
Sapporo	43.0727	141.3459	P196	46	Masatomo Fujiwara
Tsukuba-NIES	36.0513	140.1210	P176	45	Tamaki Fujinawa
Tokyo-TMU	35.6200	139.3834	P194	135	Shungo Kato
Fukuoka	33.5491	130.3660	P199	55	Hisahiro Takashima

Table S2: Emission inventories employed in the GEOS-Chem model simulations

Source	Inventory	Resolution	Reference
Anthropogenic			
+ Global	CEDSv2	0.5° × 0.5°	McDuffie et al. (2020)
+ Japan	REASv3.2.1	0.25° × 0.25°	Kurokawa and Ohara (2020)
Aircraft	AEIC 2019	1° × 1°	Simone et al. (2013)
Biomass burning	GFED4	0.25° × 0.25°	van der Werf et al. (2017)
Lightning	-	0.5° × 0.625°	Murray et al. (2012)
Off-line biogenic VOCs, Soil NO_x, sea salt aerosol	-	0.5° × 0.625°	Weng et al. (2020)
Off-line dust	-	0.5° × 0.625°	Meng et al. (2021)
Shipping	CEDSv2	0.5° × 0.5°	McDuffie et al. (2020)

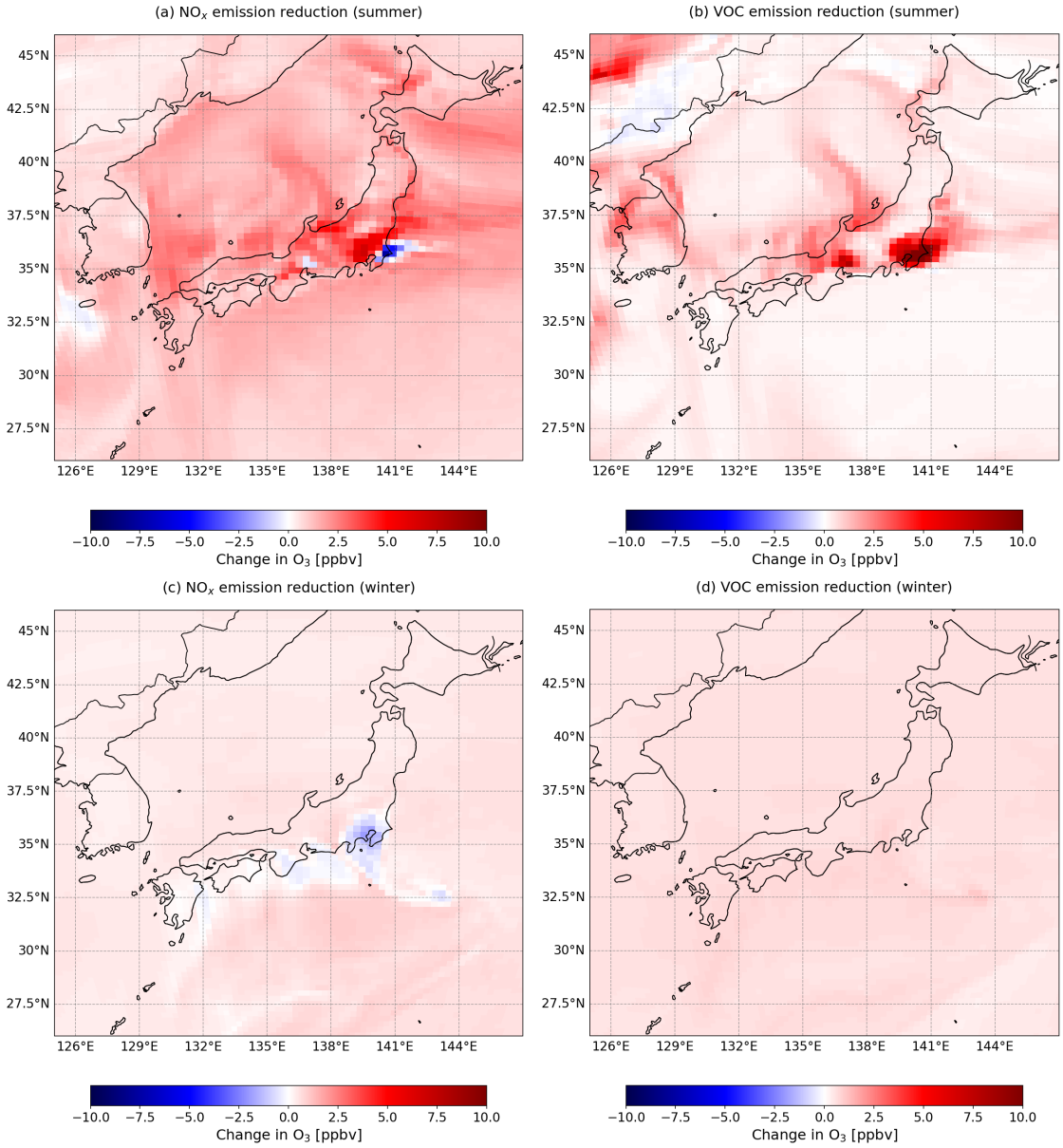

Figure S1: GEOS-Chem model simulations of changes in the surface ozone concentration at 13:00 in response to NO_x emission reduction (a, c) and VOC emission reduction (b, d). Change in O_3 is defined by subtracting Run-3 or Run-4 from Run-2. The top panels present changes in summer, while the bottom panels present changes in winter. Red and blue colors indicate positive (decrease) and negative change (increase) in the surface ozone concentration, respectively.

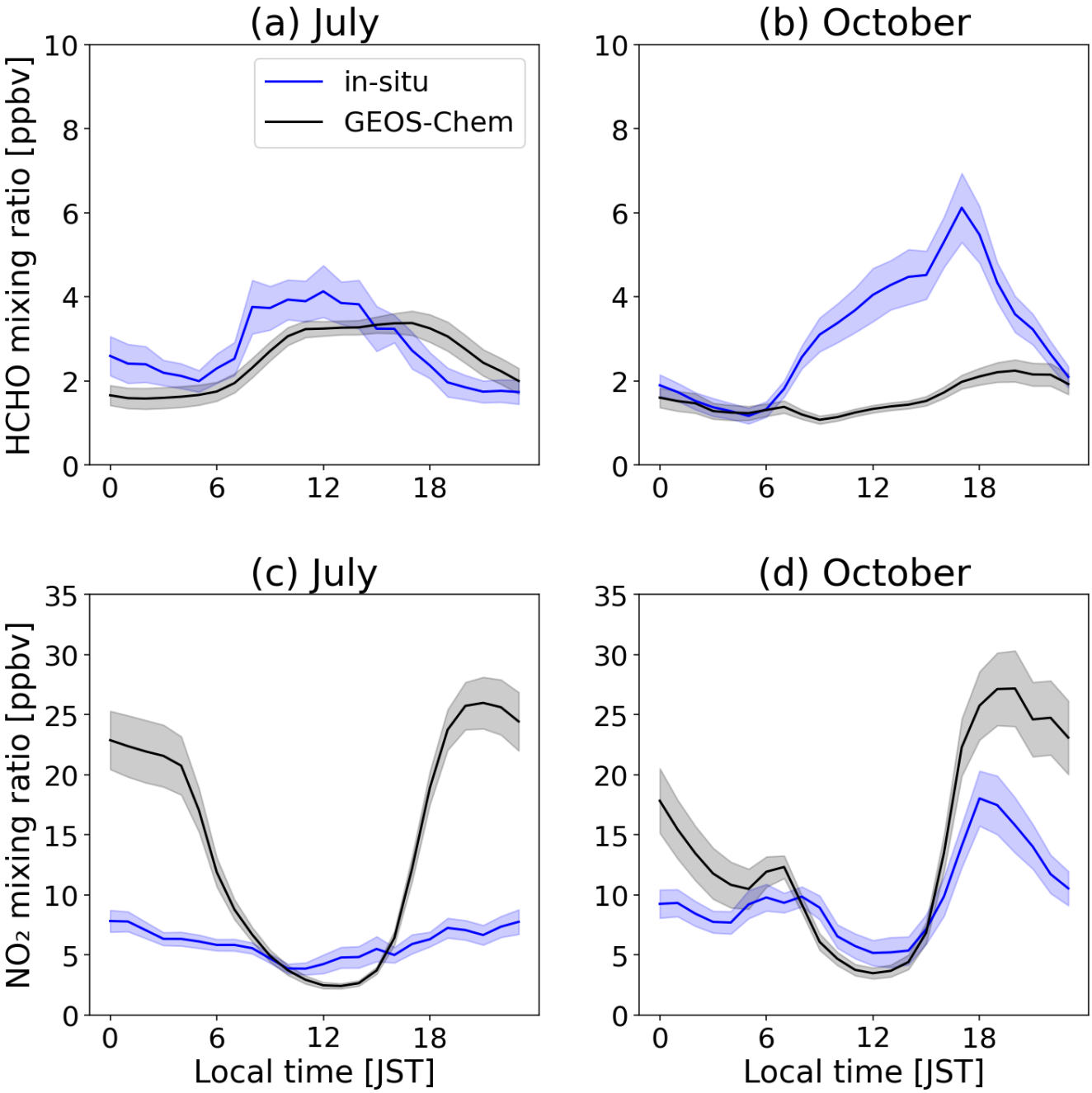

Figure S2: Diurnal cycle of the surface HCHO (top panels) and NO_2 (bottom panels) obtained from in situ measurements (blue) and GEOS-Chem simulations (black) at the Tokyo-TMU site in July (a and c) and in October (b and d) 2022. Shaded error bands indicate ±1 standard error.

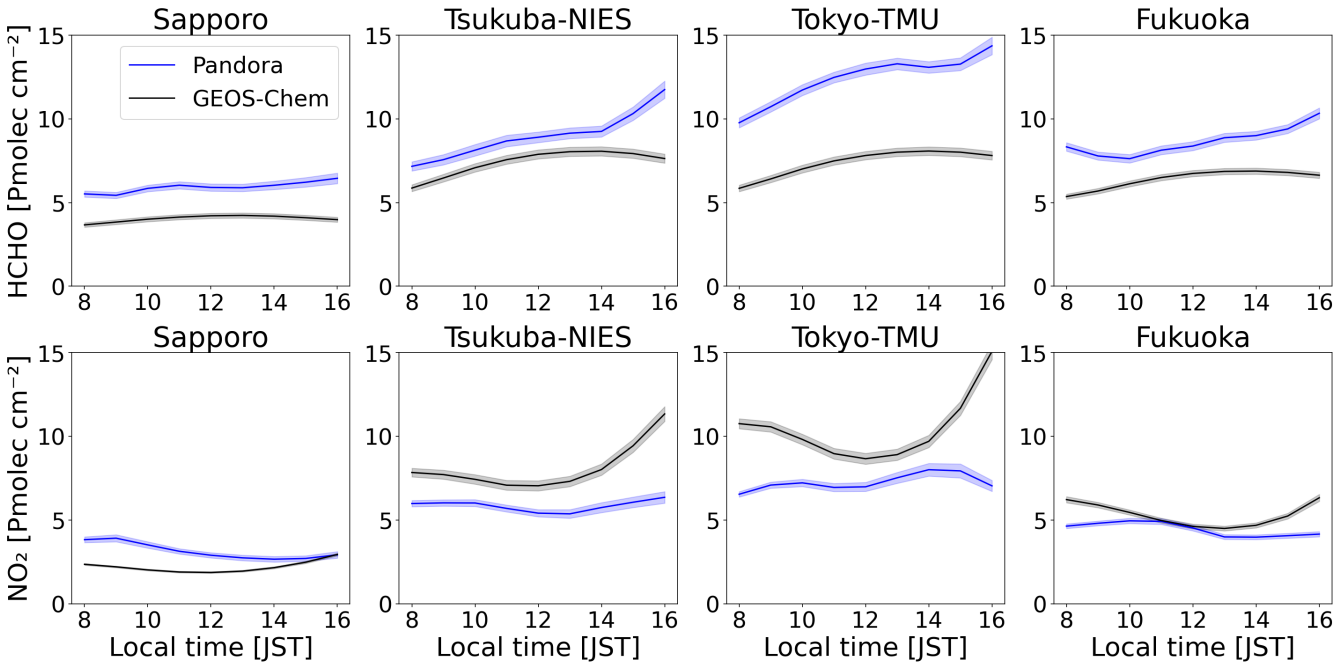

Figure S3: Diurnal variation of annual tropospheric vertical column densities of HCHO and NO_2 obtained from Pandora (blue) and GEOS-Chem model simulation (black). Shaded error bands indicate ±1 standard error.

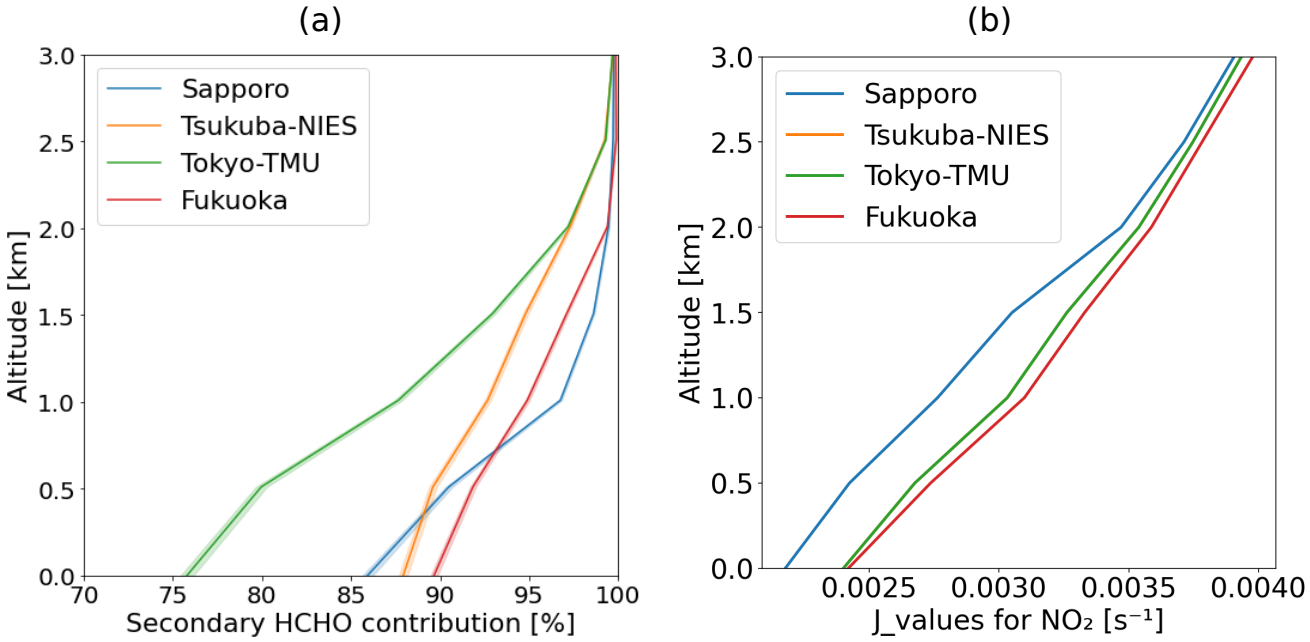

Figure S4: (a) Vertical contributions of secondary HCHO (annual mean) at the study JPN sites obtained from GEOS-Chem model. (b) Photolysis rate (J_values) for NO_2 at the study locations. Shaded error bands indicate ±1 standard error.

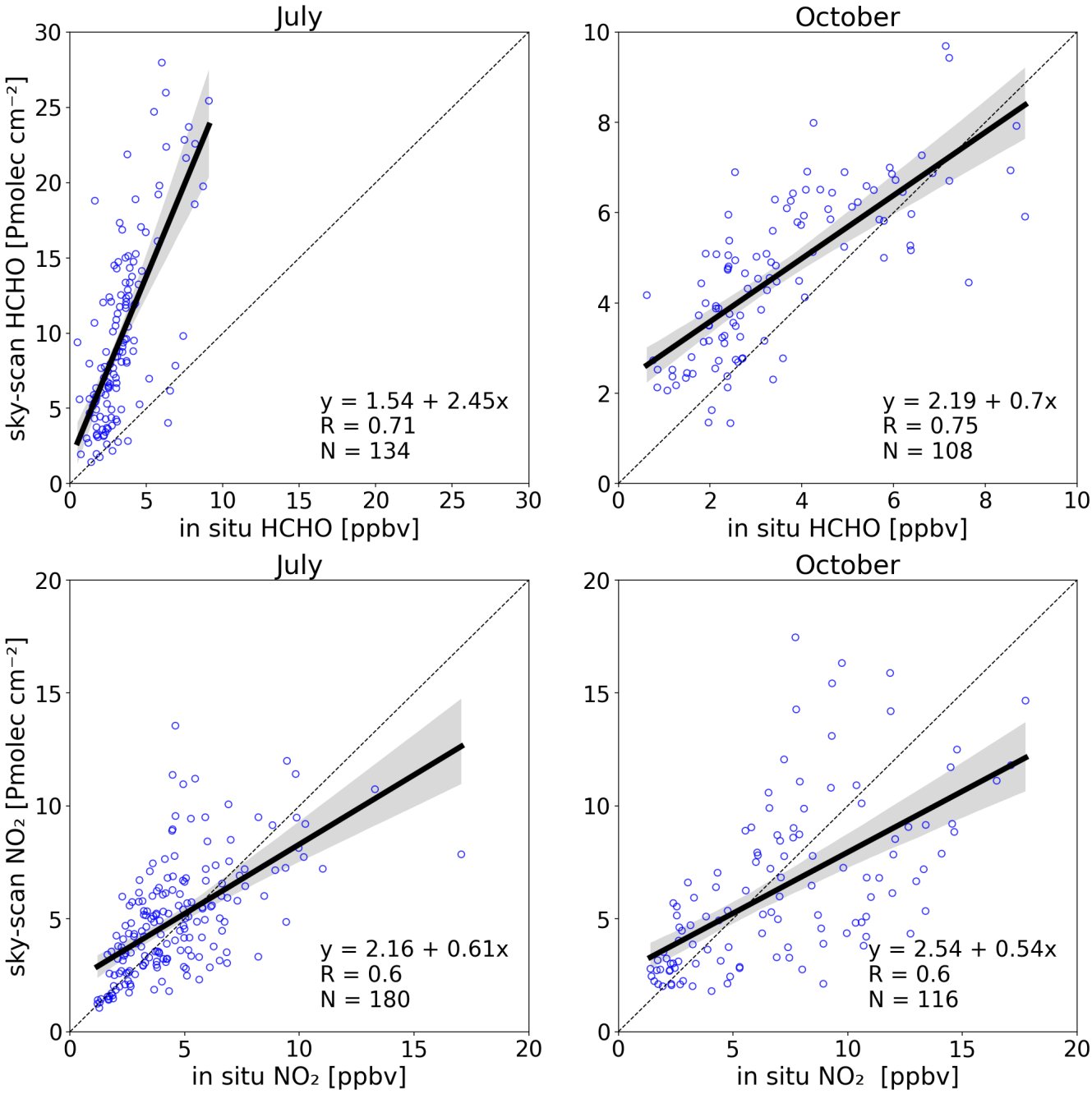

25 **Figure S5: Relationship in HCHO (top panels) and NO_2 (bottom panels) between the lower tropospheric column (Pandora sky-scan) and the surface concentrations (in situ measurements). The dashed line indicates the 1:1 line.**

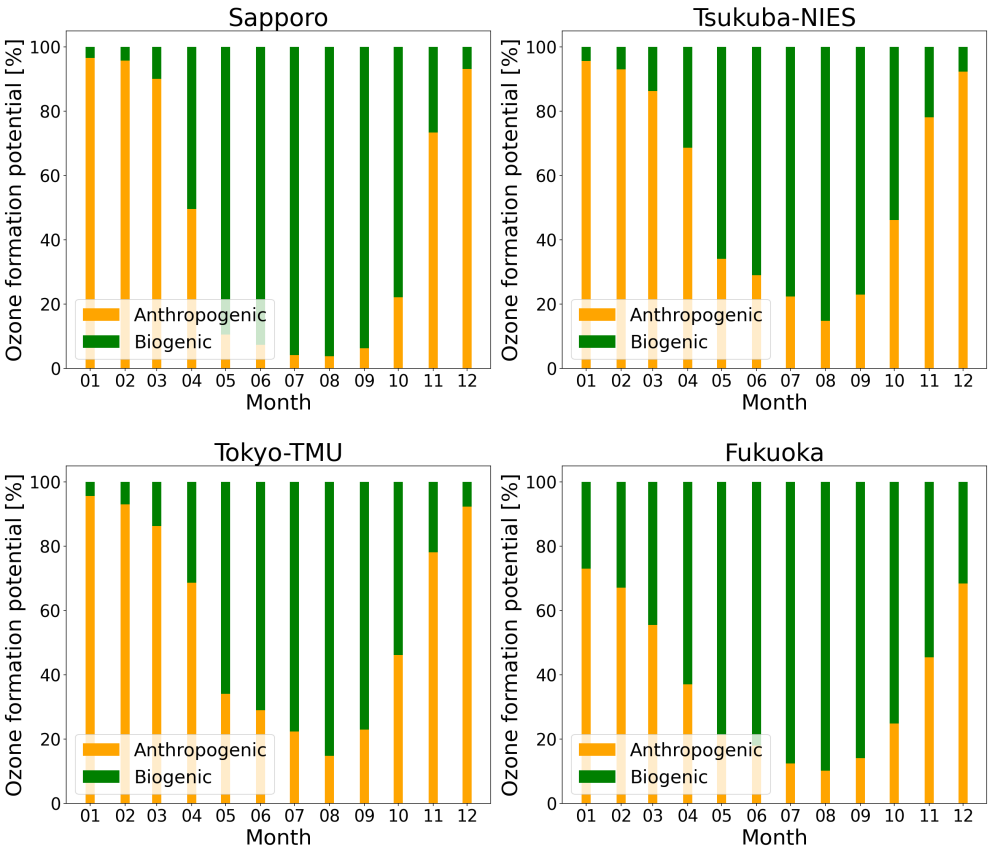

Figure S6: Biogenic and anthropogenic VOCs contributions to O_3 formation potential (OFP). OFP is estimated by multiplying VOC with maximum incremental reactivity coefficient (Carter, 1994).

30

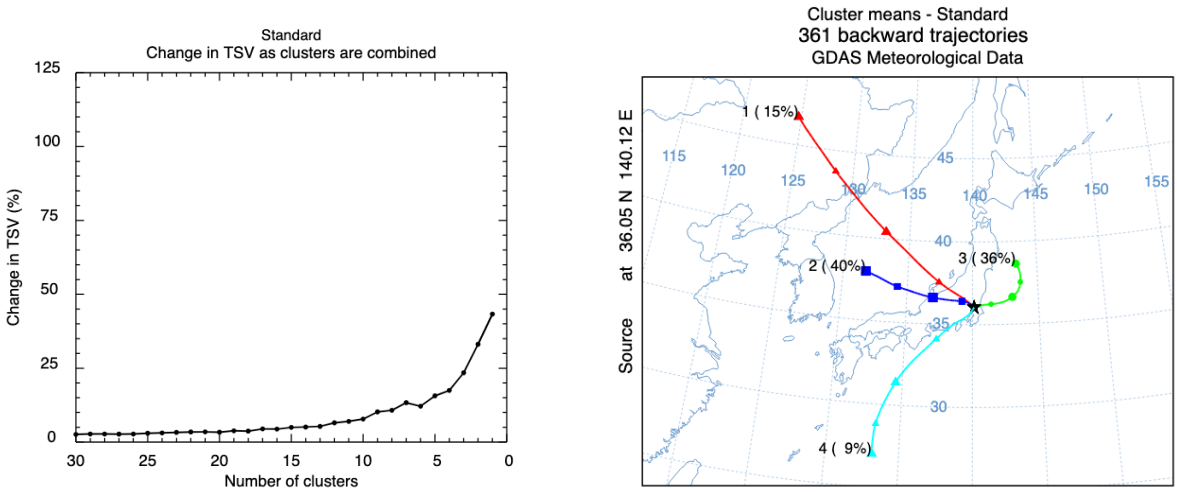

Figure S7: Cluster analysis based on the change in total spatial variance (TSV) (left panel) and cluster means (right panel) of one-year backward trajectories arriving at 13:00 at Tsukuba-NIES site using HYSPLIT model. Four clusters include c1 (red), c2 (blue), c3 (green), and c4 (cyan).

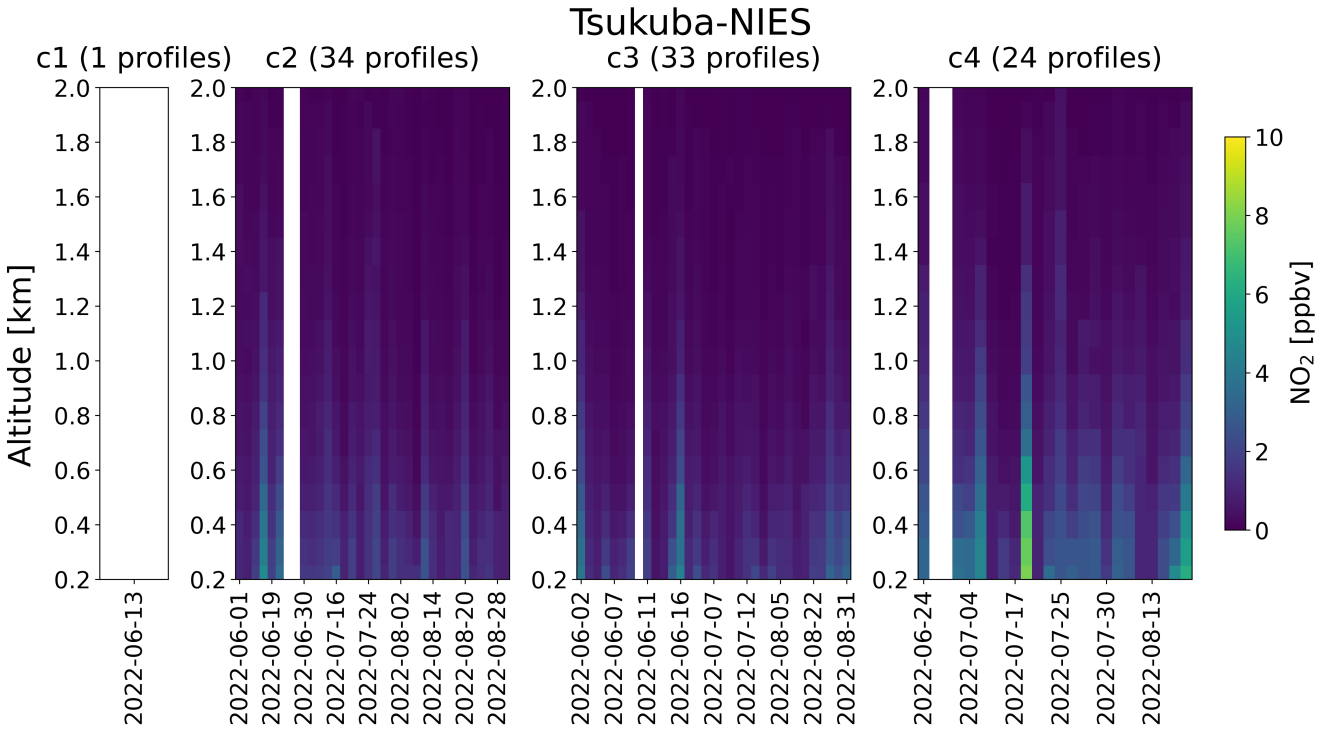

Figure S8: Vertical profiles of NO_2 during summer as a function of air mass cluster at Tsukuba-NIES.

40

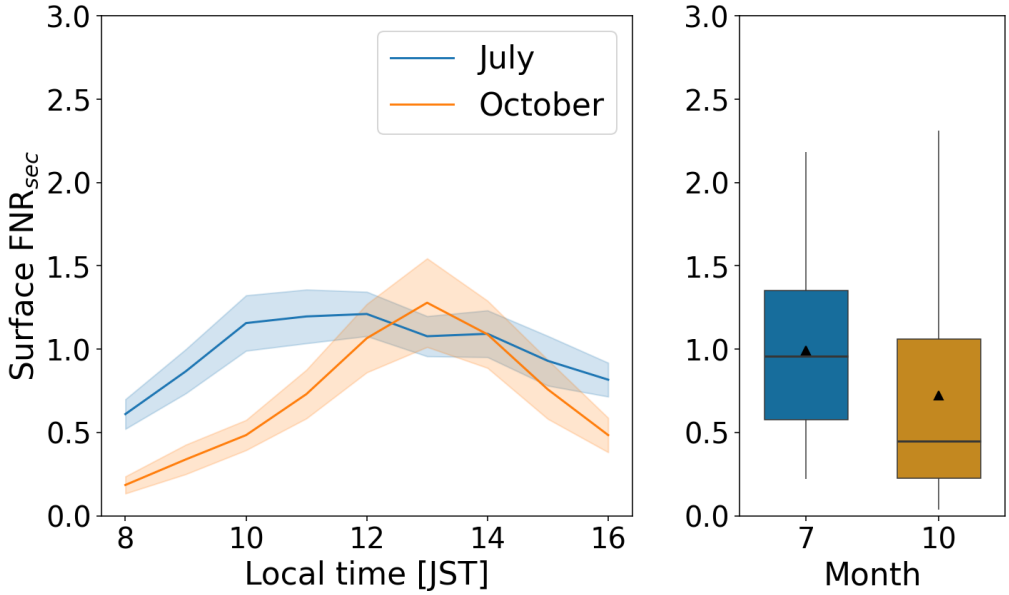

Figure S9: Variation in the surface FNR_{sec} at Tokyo-TMU. The left panel shows the diurnal cycle. Shaded error bands indicate ±1 standard error. The box plots indicate monthly FNR_{sec} (8:00-16:00), with the median (solid line) and mean (triangle).

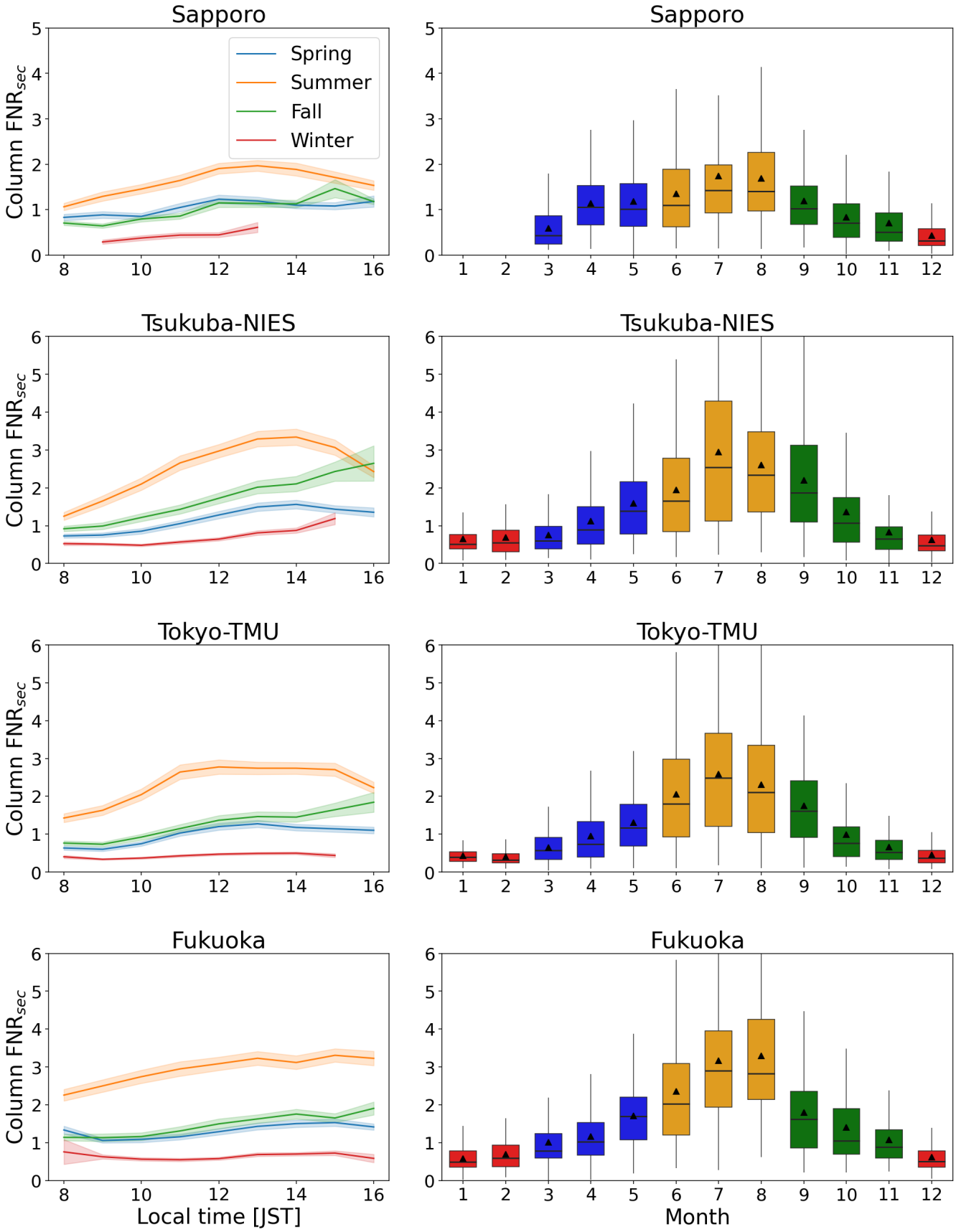

45 **Figure S10: Tropospheric column FNR_{sec} obtained from Pandora measurements at the study locations. The left columns show the diurnal cycle from 8:00 to 16:00. Shaded error bands indicate ±1 standard error. The box plots indicate the monthly column FNR_{sec} (8:00-16:00), with the median (solid line) and mean (triangle).**

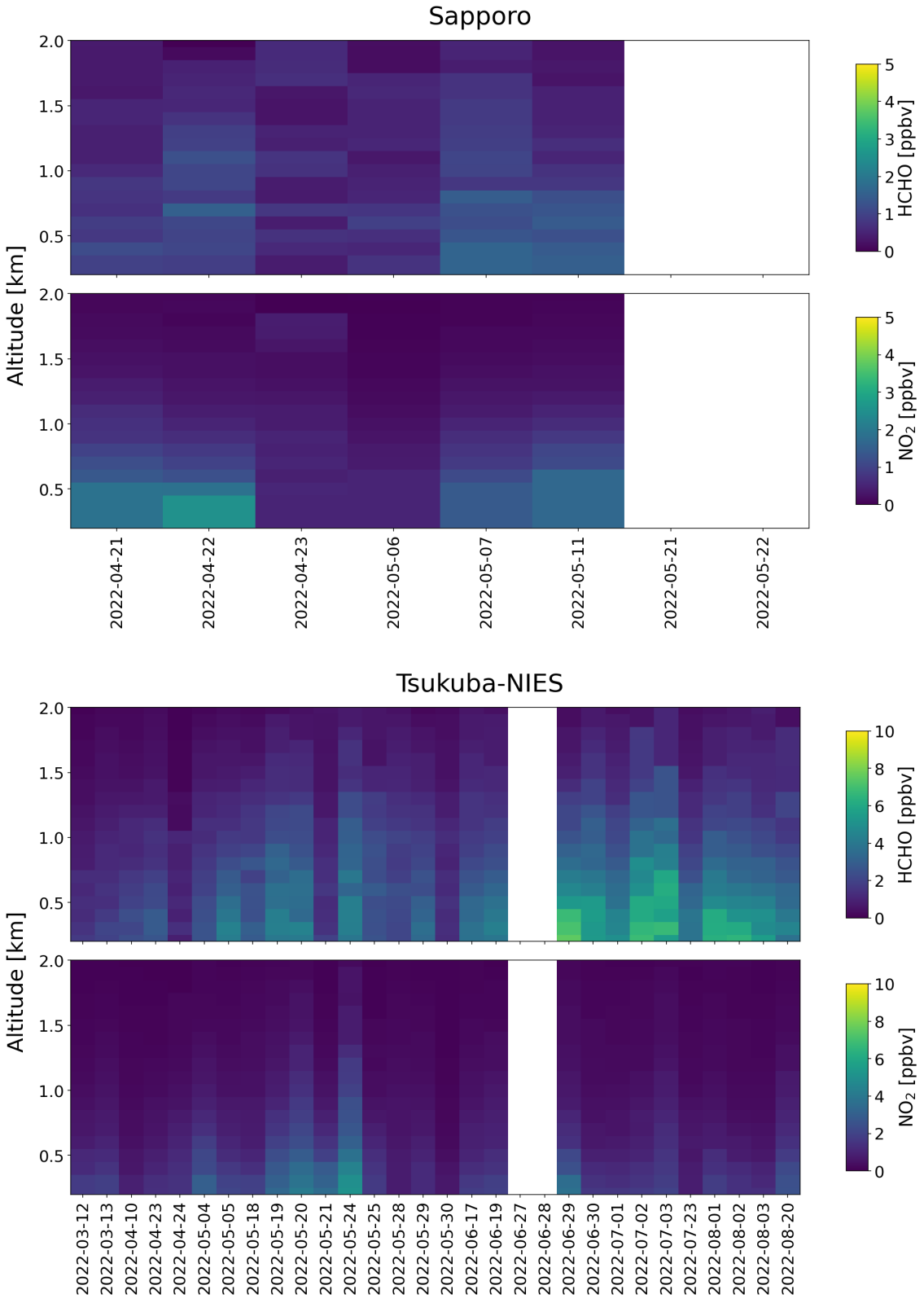

Figure S11: Vertical profiles of HCHO (top panels) and NO_2 (bottom panels) derived from the Pandora sky-scan mode at Sapporo and Tsukuba-NIES. Color bars exhibit the diurnal profiles.

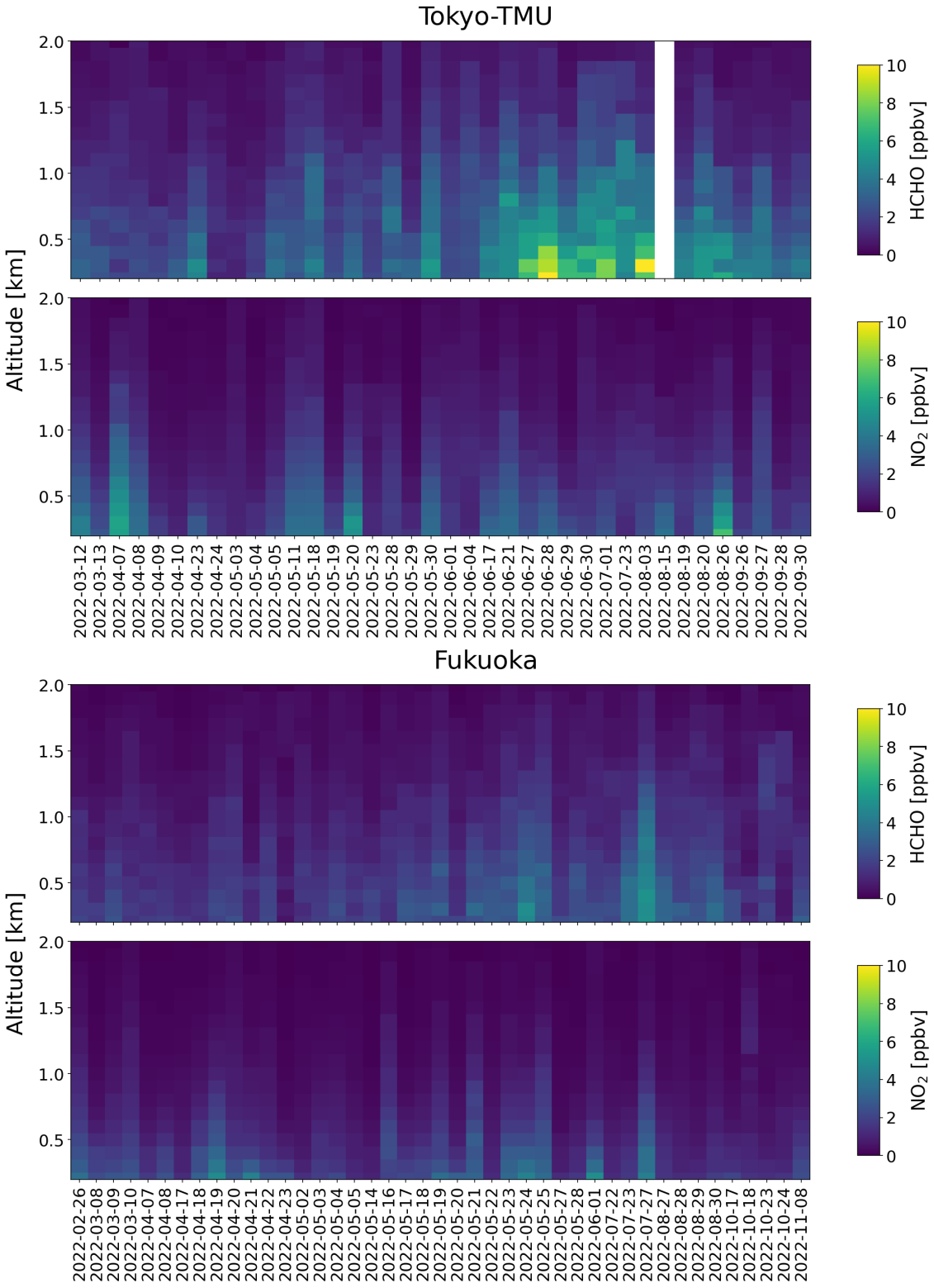

Figure S12: Vertical profiles of HCHO (top panels) and NO_2 (bottom panels) derived from the Pandora sky-scan mode at Tokyo-TMU and Fukuoka. Color bars exhibit the diurnal profiles.

References

Carter, W. P. L.: Development of Ozone Reactivity Scales for Volatile Organic Compounds, Air & Waste, 44, 881–899, https://doi.org/10.1080/1073161X.1994.10467290, 1994.

Kurokawa, J. and Ohara, T.: Long-term historical trends in air pollutant emissions in Asia: Regional Emission inventory in ASia (REAS) version 3, Atmos. Chem. Phys., 20, 12761–12793, https://doi.org/10.5194/acp-20-12761-2020, 2020.

McDuffie, E., Smith, S., O'Rourke, P., Tibrewal, K., Venkataraman, C., Marais, E., Zheng, B., Crippa, M., Brauer, M., and Martin, R.: CEDS_GBD-MAPS: Global Anthropogenic Emission Inventory of NOx, SO_2, CO, NH_3, NMVOCs, BC, and OC from 1970-2017 (2020_v1.0), https://doi.org/10.5281/ZENODO.3754964, 2020.

Meng, J., Martin, R. V., Ginoux, P., Hammer, M., Sulprizio, M. P., Ridley, D. A., and Van Donkelaar, A.: Grid-independent high-resolution dust emissions (v1.0) for chemical transport models: application to GEOS-Chem (12.5.0), Geosci. Model Dev., 14, 4249–4260, https://doi.org/10.5194/gmd-14-4249-2021, 2021.

Murray, L. T., Jacob, D. J., Logan, J. A., Hudman, R. C., and Koshak, W. J.: Optimized regional and interannual variability of lightning in a global chemical transport model constrained by LIS/OTD satellite data, J. Geophys. Res. Atmos., 117, 2012JD017934, https://doi.org/10.1029/2012JD017934, 2012.

Simone, N. W., Stettler, M. E. J., and Barrett, S. R. H.: Rapid estimation of global civil aviation emissions with uncertainty quantification, Transp. Res. D Trans. Environ., 25, 33–41, https://doi.org/10.1016/j.trd.2013.07.001, 2013.

Van Der Werf, G. R., Randerson, J. T., Giglio, L., Van Leeuwen, T. T., Chen, Y., Rogers, B. M., Mu, M., Van Marle, M. J. E., Morton, D. C., Collatz, G. J., Yokelson, R. J., and Kasibhatla, P. S.: Global fire emissions estimates during 1997–2016, Earth Syst. Sci. Data, 9, 697–720, https://doi.org/10.5194/essd-9-697-2017, 2017.

Weng, H., Lin, J., Martin, R., Millet, D. B., Jaeglé, L., Ridley, D., Keller, C., Li, C., Du, M., and Meng, J.: Global high-resolution emissions of soil NOx, sea salt aerosols, and biogenic volatile organic compounds, Sci Data, 7, 148, https://doi.org/10.1038/s41597-020-0488-5, 2020.